



# Evolution of interfacial defects and energy losses during aging of organic photovoltaics

Peng Liu<sup>a</sup>, Yisong Huang<sup>a</sup>, Zhe Wang<sup>a,\*</sup>, Wansheng Liu<sup>a</sup>, Boonkar Yap<sup>b,c</sup>, Zhicai He<sup>a,\*\*</sup>, Hongbin Wu<sup>a</sup>

<sup>a</sup> Institute of Polymer Optoelectronic Materials and Devices, State Key Laboratory of Luminescent Materials and Devices, South China University of Technology, Guangzhou, 510640, PR China

<sup>b</sup> Electronic and Communications Department, College of Engineering, Universiti Tenaga Nasional, 43000, Kajang, Selangor, Malaysia

<sup>c</sup> Institute of Sustainable Energy, Universiti Tenaga Nasional, 43000, Kajang, Selangor, Malaysia

## ARTICLE INFO

### Keywords:

Organic solar cells  
Interfacial defect state  
Recombination  
Energy loss  
Work function

## ABSTRACT

As the power conversion efficiencies of Organic Solar Cells (OSCs) approach 20 %, the stability of the device becomes an increasingly urgent issue. To enhance device stability, it is crucial to identify potential loss mechanisms. In this study, we investigated the trap-state-dependent degradation mechanism of OSCs by directly comparing devices with different hole transport layers (HTLs) that introduce distinct interfacial defect distributions. Employing electrochemical impedance spectroscopy (EIS), Fourier transform photocurrent spectroscopy (FTPS), electroluminescence quantum efficiency (EQE<sub>EL</sub>), and temperature-dependent J-V techniques, we unraveled the relationship between device degradation and interfacial trap states and energy loss in PM6:Y6 devices. A lower density of interfacial deep traps is evidently correlated with smaller non-radiative recombination losses during the aging of devices based on PEDOT:PSS. Conversely, a higher density of deep traps in aged devices with WS<sub>2</sub> interlayers and HTL-free configurations is presumed to be responsible for a significant increase in non-radiative recombination losses. The escalating deep-trap-state density in aged devices is observed to elevate carrier recombination, consequently deteriorating device performance. Beyond the scope of the energy balance theory, an additional factor, probably attributed to the change in the work function of ITO, was found to contribute significantly to energy loss in aged cells, particularly in HTL-free devices. These results highlight the potential for improving device stability via interface engineering.

## 1. Introduction

In the last decade, substantial advancements in materials and device architecture optimization have propelled the power conversion efficiency (PCE) of Organic Solar Cells (OSCs) towards 20 % [1–3]. While this significant progress has been achieved in enhancing device efficiency, the stability of these devices has emerged as a critical research focus [4–7]. Defects and disorder states within the devices are recognized as major contributors to device degradation. Therefore, investigating defects and disorder states is crucial for understanding the factors influencing device degradation and formulating strategies to enhance device performance [8]. Due to the intricate nature of microscopic regions in OSCs, studying the generation, distribution, and evolution of defects during degradation remains challenging.

Structural defects, such as grain boundaries and molecular vacancies, are known to broaden the optical band edge and influence the energy level alignment at organic/substrate interfaces, ultimately leading to device degradation [9–11]. Additionally, various interlayers, such as PEDOT [12,13], nano-functional layers [14,15], two-dimensional nanomaterials [16,17], organic dipole Interlayers [18, 19] are employed on ITO to minimize the contact barrier between the electrode and the active layer, thereby improving device performance. It is commonly accepted that interfacial defect states in different interlayers can vary significantly, impacting device stability. For instance, Transition Metal Dichalcogenides (TMDs), while demonstrating potential to enhance initial device performance, are found to possess a high level of interfacial defect states due to poor film uniformity and a large number of surface vacancies [20,21], posing a threat to long-term

\* Corresponding author.

\*\* Corresponding author.

E-mail addresses: [wangz@scut.edu.cn](mailto:wangz@scut.edu.cn) (Z. Wang), [zhicaihe@scut.edu.cn](mailto:zhicaihe@scut.edu.cn) (Z. He).

stability. Defect states originating from electrode-organic interface degradation can result in severe charge recombination, leading to a drop in  $V_{OC}$  (open-circuit voltage) and  $FF$  (fill factor) [22]. Despite reported passivation strategies for surface defects [23–26], which can facilitate charge extraction and suppress recombination, a comprehensive understanding of the role of interfacial defect states in the degradation of high-performance OSCs is still lacking.

This work focuses on the role of interfacial defects and their evolution in the long-term stability of PM6:Y6 devices derived from different substrates (PEDOT:PSS, WS<sub>2</sub>, and HTL-free). Defect states and related band tails are investigated using C- $\omega$  and FTPS to comprehend interband transitions during device degradation under various interface conditions. The contribution of the Urbach band tail to device performance is examined through hole transport characteristics at low temperatures, confirming the impact of trap states induced by interfacial defects near the energy level of the donor on  $V_{OC}$  degradation. Comprehensive analysis reveals a correlation between the drop in  $V_{OC}$  and increased deep trap states during degradation for all devices. Notably, an energy loss beyond the energy balance theory, probably attributed to a change in work function, is found to be a significant factor, especially for HTL-free devices. These results underscore the potential for enhancing device stability through interface engineering.

## 2. Results and discussion

### 2.1. Photovoltaic and photoelectric properties

To elucidate the degradation behaviors of Organic Solar Cells (OSCs), we initially measured the time-dependent evolution of Power Conversion Efficiency (PCE), Open-Circuit Voltage ( $V_{OC}$ ), Short-Circuit Current ( $J_{SC}$ ), and Fill Factor ( $FF$ ) in ITO/HTL/PM6:Y6/PDINO/Ag devices. Fig. 1 illustrates distinct degradation behaviors for the three types of OSCs. The control device without Hole Transport Layers (HTLs) exhibits rapid degradation within the first 72 h. Notably, while the Short-Circuit Current ( $J_{SC}$ ) of the fresh device without HTLs closely matches that of the other two devices, its Open-Circuit Voltage ( $V_{OC}$ ) is significantly lower at 0.48 V. This marked decrease in  $V_{OC}$  can be attributed to the substantial energy offset between the electrode and the active layer,

highlighting the crucial role of the charge transport layer in adjusting the electrode's work function. After aging for approximately 800 h, the  $V_{OC}$  of the device without HTLs experiences a substantial decline from 0.49 V to 0.24 V, while its  $J_{SC}$  only reduces by about one-fifth. On the other hand, the device derived from WS<sub>2</sub> also exhibits inferior long-term stability compared to that from PEDOT:PSS, particularly in terms of  $V_{OC}$  and  $FF$ . This observation prompts the speculation that factors beyond the energy balance theory contribute to the significant  $V_{OC}$  loss during device aging, a topic we will delve into in the subsequent discussion.

As previously reported, the substantial difference in the stability of these devices can be primarily attributed to complex factors such as morphology evaluation, interface attenuation, and electrode degradation [5,27]. The varying degree of voltage loss is suggested to correlate with differences in energetic disorder and defect states [28]. When examining the impact of trap states, the ideality factor ( $n_{id}$ ) is often considered. The  $n_{id}$  can be extracted by evaluating the slope of the exponential region from the dark current-voltage curves, as expressed by the following equation (1) [29,30]:

$$n_{id}(V) = \left( \frac{k_B T}{q} \frac{d \ln \frac{J(V)}{1mA cm^{-2}}}{dV} \right) \quad (1)$$

where  $k_B$  is Boltzmann's constant,  $T$  is temperature and  $q$  is the elementary charge. As shown in Fig. 2e-g, the  $n_{id}$  for all devices are close to 2, indicating that the mid-gap states may dominate the recombination [31]. For comparison, all  $n_{id}$  values in the minimum of the curves were considered, except for the device without HTL after approximately 792 h of storage, where the data is unavailable due to limited slope. Despite the consistent  $n_{id}$  values, as shown in Fig. 2e-g, no clear relationship between time-dependent evaluations of  $n_{id}$  and device performance can be observed. This lack of correlation may stem from the fact that variations in shunt and series resistance could exert a more pronounced influence on the performance of aging devices. Consequently, a more comprehensive analysis of interface and bulk resistance is necessary to gain insights into device performance.

To comprehend the relationship between interfacial features and device performance, we conducted electrochemical impedance spec-

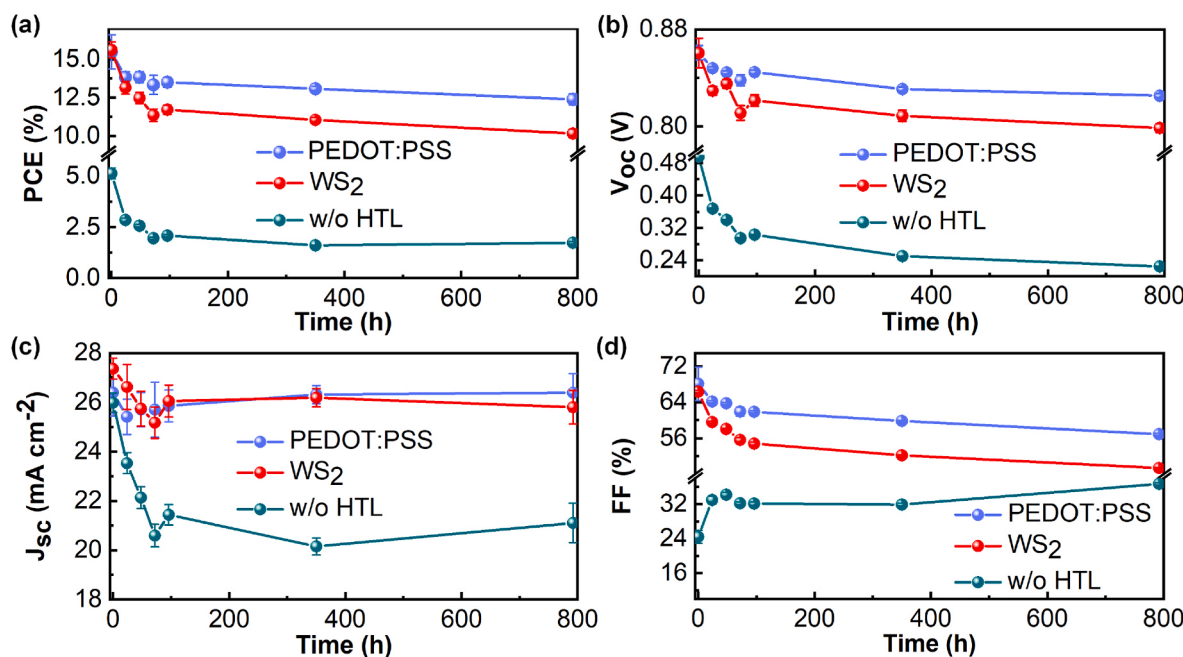


**Fig. 1.** Changes in (a) PCE, (b)  $V_{OC}$ , (c)  $FF$ , (d)  $J_{SC}$  with respect to the OSCs of PEDOT:PSS, WS<sub>2</sub> and without HTL. During the illumination test, the intensity of solar simulator was adjusted with a same reference silicon cell to produce the same test condition. During the aging process, the encapsulated devices are stored in a Nitrogen glove box at 25 °C without moisture, oxygen and light.

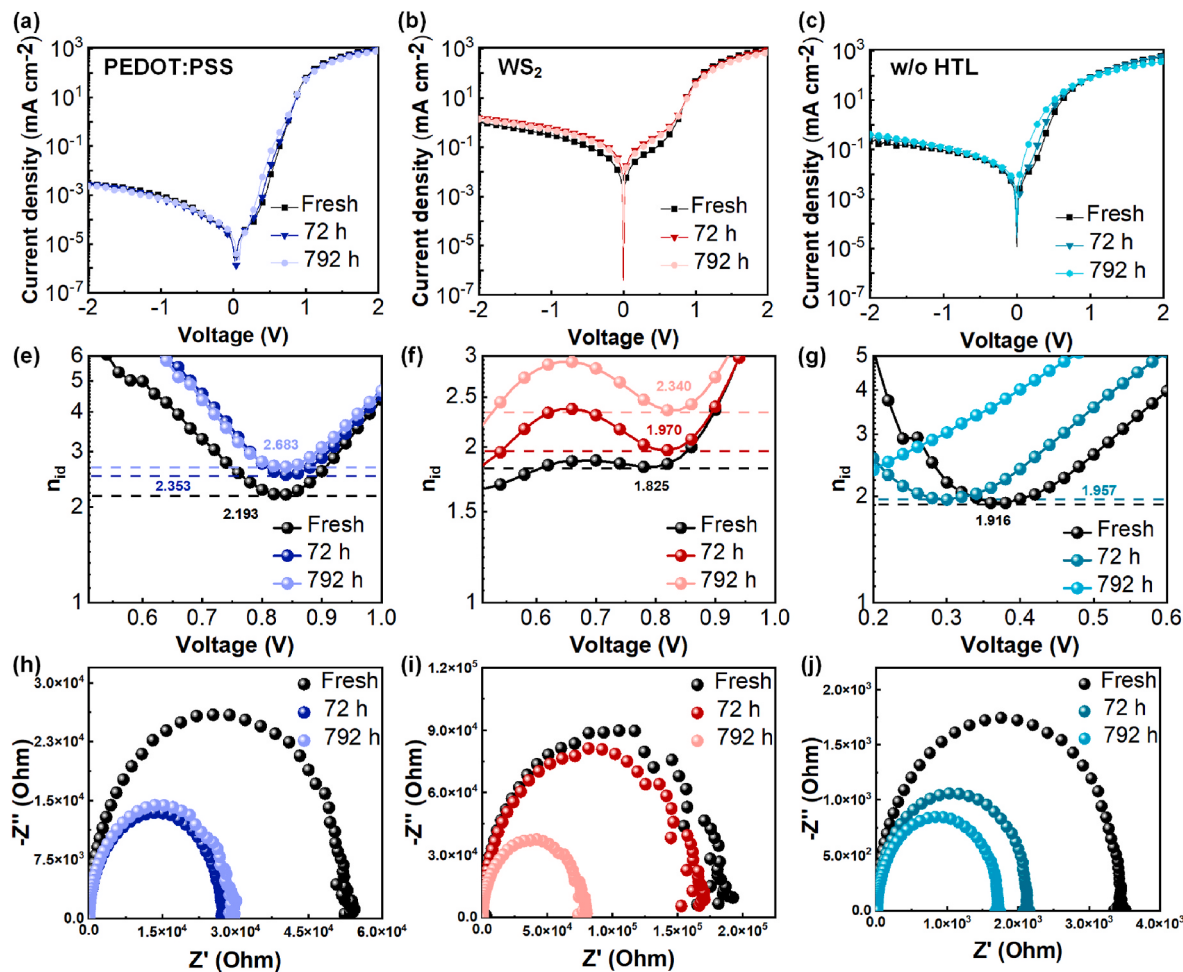


**Fig. 2.** Comparison of the devices of PEDOT:PSS, WS<sub>2</sub> and w/o HTL, respectively. (a)–(c) Current density-voltage (J-V) characteristics measured in the dark. (d)–(g) Ideality factor extracted from the J-V curves according to equation (1). (h)–(j) Nyquist plots of the OSCs.

troscopy (EIS) measurements in the dark while applying a bias voltage equal to the  $V_{OC}$  of the OSCs. Nyquist plots, as shown in Fig. 2h-j, were simulated using the Garcia-Belmonte series model, as depicted in Fig. S1 [32]. In our simulation, CPE<sub>1</sub>-Ts were obtained from the plateau regime of capacitance-frequency measurements of cells under negative bias. The simulated Nyquist plots exhibit nearly perfect matching with the measured results over a wide frequency range for all cells, validating the effectiveness of the equivalent circuit. Simulation parameters are summarized in Table 1, and all Constant Phase Elements (CPE-Ps) are between 0.9 and 1. the resistance and chemical capacitance of the active

layer should be connected in parallel way [33]. Interface resistances ( $R_1$ ) for fresh devices with ITO/PEDOT:PSS, ITO/WS<sub>2</sub>, and bare ITO were estimated to be 76, 45, and 196.9 Ω, respectively. These results suggest that the active layer of the device without an interface cannot form a good ohmic contact with the electrode, potentially impacting charge transport. Throughout the aging process,  $R_1$  of cells with interfaces gradually increases, while that of the bare ITO device decreases. This indicates that charge transport might not be a crucial factor affecting the performance degradation of the bare ITO device during degradation. Since  $R_2$  is closely related to charge recombination in the active layer, a higher positive bias makes charge recombination more likely, leading to a smaller  $R_2$ . As seen in Table 1,  $R_2$  values for all measured data align with this rule, except for the data of the bare ITO device after 72 h of aging. Notably, despite  $R_2$  almost doubling, the open-circuit voltage reduces from 0.49 V to 0.24 V, suggesting that this substantial  $V_{OC}$  reduction seems unrelated to the active layer. Furthermore, the carrier transition time ( $\tau_{avg}$ ), associated with charge recombination, can be obtained using the following equation [34]:

$$\tau_{avg} = R \times C \quad (2)$$

where  $R$  and  $C$  represent the resistance and chemical capacitance of the active layer, respectively. The obtained  $\tau_{avg}$  values for fresh devices are comparable to other efficient organic solar systems [34,35]. The decreasing trend of  $\tau_{avg}$  with increasing device aging confirms that recombination in the active layer increases over time for all types of devices. This increased recombination may arise from both the bulk and the interface. An exception is observed in the bare ITO device after 792 h

**Table 1**

Device parameters used to simulate the measured Nyquist plots of Fig. 2 using the equivalent circuit of Fig. S1.

Anode electrode	Type	$R_s$ [Ω]	$R_1$ [Ω]	CPE <sub>1</sub> -T [nF]	$R_2$ [Ω]	CPE <sub>2</sub> -T [nF]	$\tau_{avg}$ [μs]
ITO/PEDOT: PSS	Fresh	13.2	76	1.38	223.5	12	2.68
	72 h	16.8	47.5	1.45	77.5	29.8	2.31
	792 h	17.8	173	2.2	51	28	1.43
ITO/WS <sub>2</sub>	Fresh	18.5	45	1.4	115	16	1.84
	72 h	18	51	1.6	99	17.5	1.73
	792 h	13.8	172	2.3	59	18.5	1.09
ITO	Fresh	5.5	196.9	1.65	266.5	0.38	0.102
	72 h	5.6	175.2	1.9	529.4	0.17	0.09
	792 h	1	82.2	26.77	34.7	18822	653.1

of aging.  $\tau_{\text{avg}}$  rises to an unusually large value of 653.1  $\mu\text{s}$  due to the substantial  $CPE_2\text{-T}$  value of 18822 nF. This anomaly is likely attributable to the presence of numerous trap states in the device, which capture and release carriers at a slow rate, resulting in a virtual high carrier lifetime. This suggests that trap states can account for differences in device recombination, a hypothesis further supported by subsequent studies on trap states.

## 2.2. Disorder and defect states

To check the possible influence of the active layer properties on the device stability, FTPS is employed to evaluate the effect of the energetic disorder between the fresh and aged device on, by investigating the changes in the DOS between the fresh aged OSCs. The absorption tail due to the density of state (DOS) within the bandgap can be studied by the ultrasensitive optical measurement techniques, including photothermal deflection spectroscopy (PDS) [36] and Fourier transform photocurrent spectroscopy (FTPS) [37]. These techniques offer feasible ways to study the physical and chemical properties of defect states in OSCs. Although recent paper noted that it's hard to distinguish the FTPS-EQE features of different D/A interface compare to different acceptor-rich domains [38], we believe that the impact of change in D/A interfaces on device stability cannot be ignored. First, reduction of energy disorder and trap states will benefit from the optimization of the morphology, which can be directly reflected in the Eu. Second, the chemical interaction between the interfacial layers during aging should not be ignored, which may change the D/A interface. The effects of energetic disorder are often described by exponential or Gaussian DOS models to analyze the physical electronic structure [38–40]. In the analytical model of Gaussian distribution, energetic disorder lowers the  $V_{\text{OC}}$  with  $\sigma^2/k_B T$  term [41]. In the exponential model, the width of the DOS tail can be interpreted by the Urbach energy ( $E_U$ ), extractable from the low photon energy regime of the External Quantum Efficiency (EQE) spectra or absorption profile, given by  $\text{EQE}(E) \propto a(E) \propto e^{-\frac{E-E_g}{E_U}}$ , where  $E$  is photon energy and  $E_g$  is the optical gap of the active layer [42,43]. All fresh devices in this study exhibit similar  $E_U$  values ranging from 27.64 meV to 29.59 meV, as shown in Fig. 3a. After aging, the  $E_U$ s in all devices increases slightly but remains quite similar, ranging from 34.73 meV to 36.48 meV, as illustrated in Fig. 3b. Since the small change in  $E_U$  should have a negligible impact on  $V_{\text{OC}}$ , the larger change in the  $V_{\text{OC}}$  of the devices derived from bare ITO and WS<sub>2</sub> could be a result of decreased carrier concentration due to charge recombination (Fig. S2), as well as a potential increase in energy level mismatch between the substrate and the interlayer. Furthermore, the  $V_{\text{OC}}$  deficit (defined as  $E_g/q - V_{\text{OC}}$ ) can be related with  $E_U$  to analyses the possible degradation features in devices as shown Fig. S3. The  $V_{\text{OC}}$  deficit and the slope are both largest in the device derived from bare ITO compared to the others, consistent

with the significant drops in both open-circuit voltage and short-circuit current after aging. Therefore, it seems reasonable to exclude the influence of active layer properties on the larger degradation of  $V_{\text{OC}}$ .

To investigate the influence of the density distribution of interfacial trap states on device performance, the trap density of states (tDOS) in the three devices is explored through capacitance-frequency measurements during the device aging processes. As shown in Fig. 4a-c, although all three devices exhibit similar tDOS distributions within the instrumental test limitations, some small differences in details are observed.

The tDOS above 0.5 eV increases sequentially in both fresh and aged devices derived from PEDOT:PSS, WS<sub>2</sub>, and bare ITO, indicating distinct trap distributions in devices with different interlayers. As the electronic states are detected by capacitance-frequency measurements, the measured trap distribution originates from not only the active layer but also the electrodes and their interfaces [41]. Moreover, when fitting the Gaussian distribution law, the tDOS below 0.4 eV in different devices show different distribution characteristics before and after aging. The tDOS with energy below 0.4 eV exhibits a peak around 0.28 eV for the aged device based on PEDOT:PSS, which is higher than that of the fresh device (0.22 eV). However, the energy of the tDOS peak decreases in the device derived from WS<sub>2</sub> or remains almost the same in the aged device derived from bare ITO. Since it has been reported in the literature that deep traps in the photoactive layer also affect the nonradiative energy loss [44]. To rule out of the interference from the interaction between the top electrode and the active layer, we use the same electron transport layer PDINO in all devices. As indicated by the tDOS study as shown in Fig. 4a-c, device with WS<sub>2</sub> and control devices without HTL show an increase in deep traps, and PEDOT:PSS mainly shows an increase in shallow traps. More traps located at lower energy could possibly contribute to the lower activation energy, thus reducing the energy of charge trapping and de-trapping, as will be discussed below.

To assess the impact of the tDOS distribution below 0.4 eV on device charge transportation, temperature-dependent hole mobility measurements with the structure of ITO/HTL/PM6:Y6/MoO<sub>3</sub>/Ag from 80 K to 300 K are employed. As shown in Fig. 4d-f, in the high-temperature region (200–300 K), the hole mobility of all devices decreases rapidly as the temperature drops, consistent with the Gaussian DOS for the energy distribution of hopping sites [45]. In the low-temperature regime (80–200 K), carriers are strongly bound in the band tail states, and charge transport is mainly governed by multiple trapping and de-trapping of holes [46]. The activation energy ( $E_a$ ) which indicates the trapping energy of carriers can be evaluated according to  $\mu = \mu_0 \exp\left(-\frac{E_a}{k_B T}\right)$ , where  $\mu$  is mobility [47]. At lower temperatures, free carriers preferentially fill the deep band-tail states, including the shallow trap states, and the bound holes in shallow traps become free only after being thermally activated to more favorable electronic states. Therefore, a

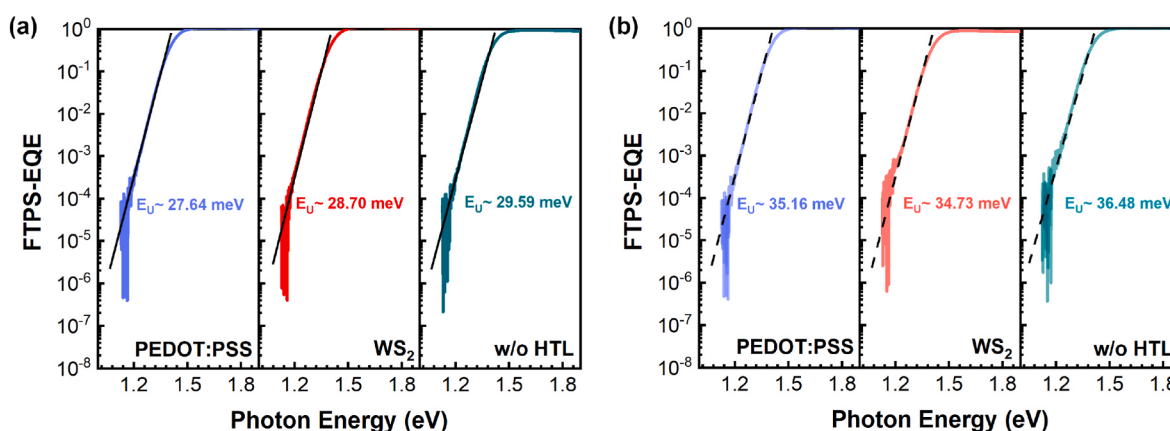
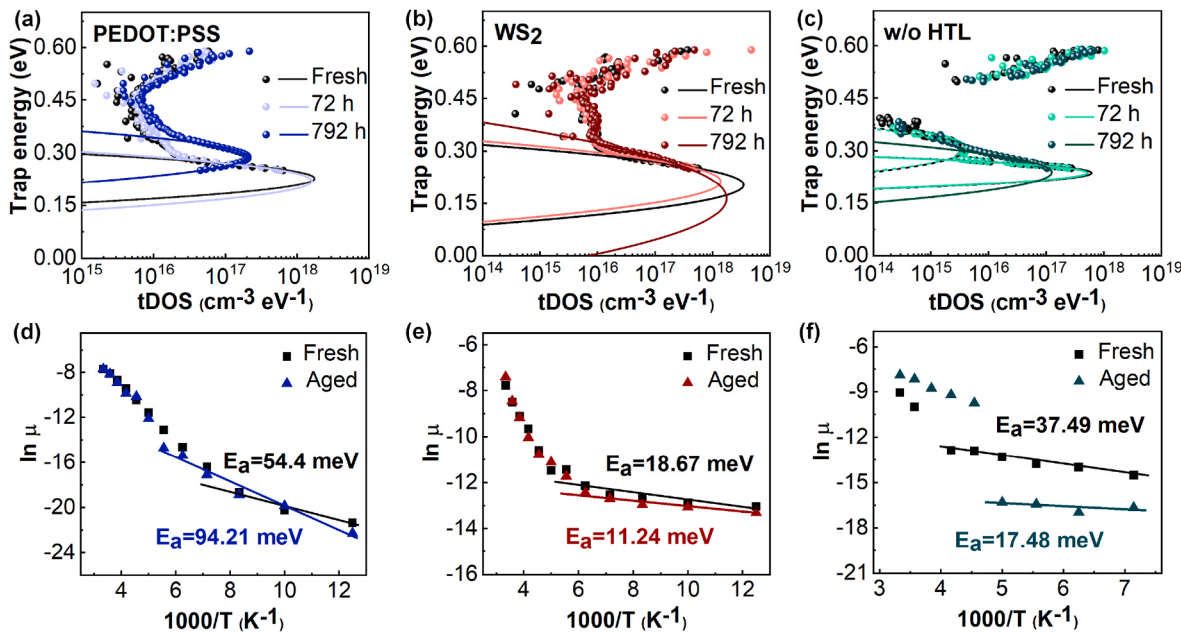


Fig. 3. FTPS-EQE spectrum of (a) fresh and (b) aged devices based on PEDOT:PSS, WS<sub>2</sub> and w/o HTL.



**Fig. 4.** The tDOS spectra of devices for different periods of time for (a) PEDOT:PSS, (b) WS<sub>2</sub>, (c) w/o HTL devices. The Gaussian fits to these devices are based on  $g(E) = \frac{N}{\sqrt{2\pi}\sigma} \exp \left[ -\frac{(E-E_0)^2}{2\sigma^2} \right]$ , where  $N$  is the total density of trap states,  $\sigma$  is the width of Gaussian and  $E_0$  is the center of the trap states distribution. Temperature dependent mobility of fresh and aged devices, the mobility versus temperature curves in logarithmic coordinates of device derived from (d) PEDOT:PSS, (e) WS<sub>2</sub>, (f) w/o HTL.

lower energy of the trap distribution should result in a smaller  $E_a$ . The smaller  $E_a$  observed in both fresh and aged devices based on WS<sub>2</sub> and bare ITO indicate a lower distribution of trap states in these devices. Importantly, the  $E_a$  of the PEDOT:PSS-based device increases from 54.4 meV to 94.21 meV after aging, while that of the WS<sub>2</sub> and bare ITO-based devices decreases from 18.67 meV to 11.24 meV and from 37.49 meV to 17.48 meV, respectively. These results align well with the trends in trap state evolution in the devices, as verified by tDOS studies.

### 2.3. Detailed energy loss

To assess the energy loss of the three devices during degradation, the electroluminescence (EL) spectra of the devices are studied, as shown in Fig. S4. Based on the detailed balance theory, the energy loss of OSCs is proposed to consist of three parts [48,49]:

$$\Delta E = \Delta E_1 + \Delta E_2 + \Delta E_3 \quad (3)$$

where  $\Delta E_1$  is the loss due to radiative recombination from absorption above bandgap,  $\Delta E_2$  is the additional radiative recombination and  $\Delta E_3$  is the non-radiative recombination. The last term of equation (3) can be quantitated by electroluminescence quantum efficiency (EQE<sub>EL</sub>), following  $\Delta E_3 = -k_B T \ln(\text{EQE}_{\text{EL}})$  [50]. Details of  $V_{OC}$  loss calculation is described in the Supplementary Note. The data of energy loss for fresh and aged devices are summarized in Table 2. The  $\Delta E_3$  of device with WS<sub>2</sub> changed from 0.252 to 0.263 eV, which is much higher than that of

PEDOT:PSS based device. Furthermore, the density of deep states in devices based on WS<sub>2</sub> and bare ITO is more than ten times that of the PEDOT:PSS-based device, as shown in Fig. 4. The analysis of photo-generated carrier lifetimes in the active layer indicates that mid-gap states could be responsible for accelerating nonradiative recombination in these devices. Therefore, we can deduce the relative values of mid-gap states in devices based on the value of  $\Delta E_3$ . The trend of non-radiative loss is consistent with the measured density of deep states induced by surface defects. Thus, it can be concluded that the generation of surface defects is the main factor for the increased non-radiative recombination in the degraded devices.

Surprisingly, the values of  $V_{OC}$  and  $\Delta E$  are also decreasing, which cannot be explained simply by energy band broadening as mentioned above. This is particularly prominent in the bare ITO device, which is 1.167 eV for the fresh device and 0.924 eV for the aged device. The extra voltage loss of 0.253 eV for the fresh device and 0.496 eV for the aged device could probably be attributed to the changed work function of ITO. This is reasonable because the equilibrium theory is based on the ideal case that the difference in work function between the two electrodes is equal to the band gap. The loss of open-circuit voltage will all come from recombination in the active layer and the energy cost for maintaining the balance with the built-in electric field. However, the work function of ITO is fragile compared to that of Ag. Once the work function of ITO changes, the balance relationship will be re-established in the device, leading to an immediate change in open-circuit voltage. In particular, we have investigated the work function of aging for pure WS<sub>2</sub>

**Table 2**  
Energy loss of the devices investigated in this study.

HTL	Time	$E_{gap}$	$qV_{OC}$	$q\Delta V$	$V_{OC, SQ}$	$V_{OC, Rad}$	$\Delta E_1$	$\Delta E_2$	$\Delta E_3$	$\Delta E + qV_{OC}$
PEDOT:PSS	Fresh	1.42	0.860	0.56	1.148	1.108	0.272	0.0395	0.252	1.423
	Aged	1.42	0.825	0.595	1.144	1.113	0.272	0.0325	0.253	1.382
WS <sub>2</sub>	Fresh	1.42	0.860	0.56	1.154	1.104	0.271	0.0503	0.252	1.433
	Aged	1.42	0.809	0.611	1.146	1.104	0.271	0.0435	0.263	1.386
–	Fresh	1.42	0.496	0.942	1.152	1.053	0.273	0.0990	0.299	1.167
	Aged	1.42	0.225	1.195	1.144	1.113	0.273	0.0321	0.394	0.924

All values are in eV.

films. After 2 weeks of aging of WS<sub>2</sub> stored in a nitrogen environment without encapsulation, the film work function decreased from 5.67 eV to 5.182 eV. Therefore, the additional reduction in open-circuit voltage is probably caused by the decrease in the ITO work function, which may be due to the further loss of oxygen atoms or the appearance of more surface states on the surface of ITO. Furthermore, the larger open-circuit voltage loss in the device without HTL may be the result of the greatly reduced work function of ITO when the donor contacts ITO directly.

The  $V_{OC}$  loss due to the change in electrode work function is found to be about 0.04 eV for the aged devices derived from PEDOT:PSS, which is around 4.7 % of  $V_{OC}$ . Meanwhile, the reduction in  $J_{SC}$  and FF accounts for 7.1 % and 13.3 %, respectively, compared to that of the fresh device. Obviously, even for the most stable devices, the energy loss caused by the change in electrode work function can achieve a comparable effect to that caused by the reduction in  $J_{SC}$  and FF. Therefore, the electrode work function not only plays an important role in the device structure of organic solar cells but also has a vital influence on the stability of devices.

With the above results, the influence of interfacial trap states on the time stability studied in this work can be illustrated in Fig. 5. The trap states, the band-tail states, and the work function of modified and unmodified anodes are correlated to understand the device degradation mechanism. The small change in band-tail states as well as shallow trap states has no obvious impact on  $V_{OC}$  loss. The degradation caused by surface defects is imposed by the relatively large nonradiative recombination loss, leading to a decrease in the stability of OSCs. Moreover, the upward shift of the anode work function could lead to further  $V_{OC}$  loss in the devices.

### 3. Conclusion

In conclusion, this study delves into the impact of interfacial defects in Organic Solar Cells (OSCs) on device time stability through the density of trap states distribution and evolution studies during the device aging process. Different degradation behaviors are observed in devices derived from PEDOT:PSS, WS<sub>2</sub>, and bare ITO. The mid-gap states and energy loss originating from interfaces are identified through various techniques, including C- $\omega$ , FTPS, EQE<sub>EL</sub>, and temperature-dependent J-V measurements, during the device degradation process. The distinct evolution trends of interfacial trap states are found to be responsible for the varied efficiency reduction in different devices. The significant change in nonradiative recombination in devices based on WS<sub>2</sub> and bare ITO is directly linked to their larger number of deep trap states. The reduced work function and redistributed trap density of states (tDOS) are identified as the main reasons for energy loss. This work on energy loss for the long-term performance of devices sheds light on improving

device stability through interface engineering. The findings provide valuable insights into the understanding and enhancement of the stability of OSCs, offering a foundation for further advancements in the field.

## 4. Methods

### 4.1. Materials

Unless otherwise specified, all the organic materials were purchased from purchased from Solarmer Cop. Poly(3,4-ethylenedioxythiophene) poly(styrenesulfonate)(PEDOT: PSS) was obtained from H.C starck Inc (CLEVIOS P VP AI4083). High purity WS<sub>2</sub> powder was purchased from ZhongNuo Advanced Material (Beijing)Technology Co., Ltd.

### 4.2. Device fabrication

For the fabrication of the PM6:Y6 based devices with different HTLs, ITO glass substrates were prepared by cleaning with a diluted detergent solution, deionized water, isopropanol and O<sub>2</sub>-plasma for 3 min respectively. WS<sub>2</sub> nanosheet solution was prepared according to our previously report [50]. A PEDOT:PSS solution was spin-coated onto the substrate at 3000 rpm for 30 s. The film of PEDOT:PSS was annealing at 150 °C for 15 min. A 50  $\mu$ L WS<sub>2</sub> solution was spin-coated onto substrate at 900 rpm for 30 s, followed by 5 min annealing at 60 °C. The PM6:Y6 (1:1.2, total 16 mg/mL) mixed with 0.5 % volume ratio of 1-chloronaphthalene solvent were spin-coated onto the PEDOT:PSS, WS<sub>2</sub> and bare ITO respectively at 3000 rpm for 40 s. The PDINO with the concentration of 1 mg/mL were spun on top of the active layer at 2000 rpm for 40 s. Finally, 100 nm Ag was thermally evaporated on the devices with the shadow mask area of 5.14 mm<sup>2</sup>.

### 4.3. Optoelectronic measurements

For the degradation study of OSCs, the J-V measurement was performed using Keithley 2400 Source in air mass 1.5 spectra (AM 1.5G) from solar simulator. The light intensity was calibrated by a reference solar cell (Hamamatsu S1133) which was certified by National Renewable Energy Laboratory. The EIS and C- $\omega$  measurements were performed via an Impedance Analyzer (E499A) in the dark. The dc bias was set to zero, the amplitude of the ac bias was 20 mV and in the scanning range of 20–10 [7] Hz. The electronic states of the cells are calculated using the equation  $N_T(E_\omega) = \frac{1}{qAd} \frac{V_{BI}}{kT} \frac{dC}{d\ln(\omega)}$ , where  $A$  is the area of device,  $d$  is the film thickness,  $V_{BI}$  is build-in potential, and  $E_\omega$  is the trap energy [51]. The demarcation energy,  $E_\omega$  can be obtained by  $E_\omega = kT \ln(\frac{\omega_0}{\omega})$ , where the

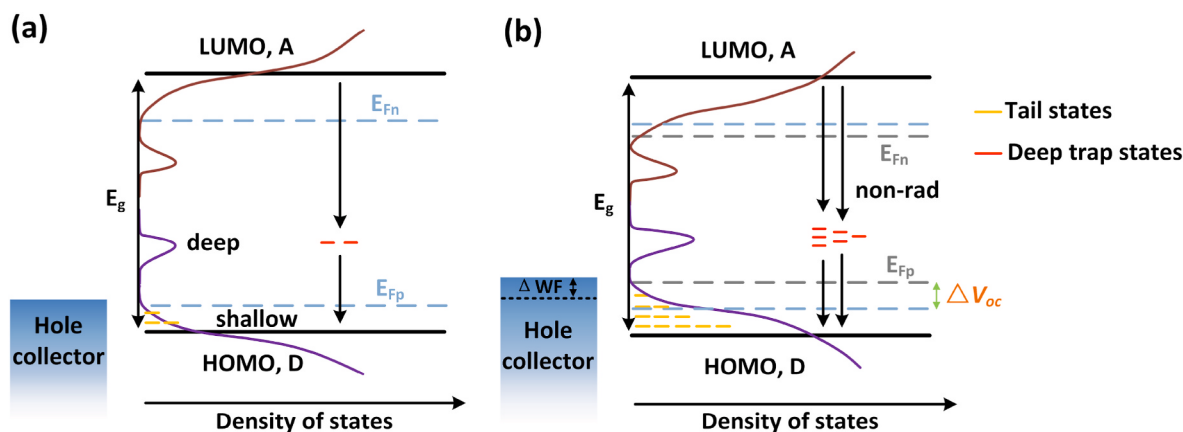


**Fig. 5.** Schematic illustration of energy diagrams which demonstrated how the tail states, mid-gap states and work function of hole collector influenced the  $V_{OC}$  of (a) fresh device and (b) aged device. After device degradation, the quasi-Fermi level of photo-generated holes shifts upward and nonradiative recombination increases, thus the  $V_{OC}$  decreases. Note that there are still electron trap states in the tail of LUMO level, but they are not emphasized in this illustration.

$\omega_0$  is the rate prefactor of thermal excitation from the trap frequency which is temperature dependence. It's assumed that  $\omega_0$  to be  $10^{-12} \text{ s}^{-1}$  according to previous report [52]. EQE test was performed by the measurement system of Enli Technology Co., Ltd. FTPS measurement was performed on a Helios pump–probe system. The system integrated with Ti:sapphire femtosecond laser amplified system and optical parametric amplifier system with 500 nm pump and NIR probe light. Temperature dependent J-V characteristics measurement was performed by optical cryostat (PHY-ST-100, Physike Technology Co., Ltd) in the temperature range of 80–300 K. EL measurement was performed by Keithley 2400 Source to obtain an injection current of 25 mA, combined with a radiation flux acquisition system with integrating sphere for signal acquisition.

### CRediT authorship contribution statement

**Peng Liu:** Methodology, Investigation. **Yisong Huang:** Data curation. **Zhe Wang:** Writing – original draft, Writing – original draft. **Wansheng Liu:** Data curation. **Boonkar Yap:** Writing – review & editing. **Zhicai He:** Writing – review & editing. **Hongbin Wu:** Writing – review & editing.

### Declaration of competing interest

The authors declare that they have no competing financial interests or personal relationships that could have appeared to influence the work reported in this paper.

### Data availability

Data will be made available on request.

### Acknowledgements

This work was financially supported by the National Natural Science Foundation of China (21733005), the China Scholarship Council, the Guangdong Science and Technology Department (2020A0505100002), the Ministry of Science and Technology of the People's Republic of China (2017YFA0206600), the 111 Project (BP0618009), the Guangdong-Hong Kong-Macao Joint Laboratory of Optoelectronic and Magnetic Functional Materials (2019B121205002), the Guangzhou Applied Basic Research Project (2023A04J1696).

### Appendix A. Supplementary data

Supplementary data to this article can be found online at <https://doi.org/10.1016/j.physb.2024.415707>.

### References

- [1] Y. Cui, Y. Xu, H. Yao, P. Bi, L. Hong, J. Zhang, Y. Zu, T. Zhang, J. Qin, J. Ren, Z. Chen, C. He, X. Hao, Z. Wei, J. Hou, Single-junction organic Photovoltaic cell with 19% efficiency, *Adv. Mater.* 33 (41) (2021) e2102420.
- [2] J. Wang, Z. Zheng, Y. Zu, Y. Wang, X. Liu, S. Zhang, M. Zhang, J. Hou, A Tandem organic Photovoltaic cell with 19.6% efficiency Enabled by light distribution control, *Adv. Mater.* 33 (39) (2021) e2102787.
- [3] Z. Zheng, J. Wang, P. Bi, J. Ren, Y. Wang, Y. Yang, X. Liu, S. Zhang, J. Hou, Tandem organic solar cell with 20.2% efficiency, *Joule* 6 (1) (2022) 171–184.
- [4] Y. Qin, N. Balar, Z. Peng, A. Gadisa, I. Angunawela, A. Bagui, S. Kashani, J. Hou, H. Ade, The performance-stability conundrum of BTP-based organic solar cells, *Joule* 5 (8) (2021) 2129–2147.
- [5] R. Sun, W. Wang, H. Yu, Z. Chen, X. Xia, H. Shen, J. Guo, M. Shi, Y. Zheng, Y. Wu, W. Yang, T. Wang, Q. Wu, Y. Yang, X. Lu, J. Xia, C.J. Brabec, H. Yan, Y. Li, J. Min, Achieving over 17% efficiency of ternary all-polymer solar cells with two well-compatible polymer acceptors, *Joule* 5 (6) (2021) 1548–1565.
- [6] J. Xiao, M. Ren, G. Zhang, J. Wang, D. Zhang, L. Liu, N. Li, C.J. Brabec, H.-L. Yip, Y. Cao, An Operando study on the Photostability of Nonfullerene organic solar cells, *Sol. RRL* 3 (7) (2019).
- [7] M. Zhang, L. Zhu, G. Zhou, T. Hao, C. Qiu, Z. Zhao, Q. Hu, B.W. Larson, H. Zhu, Z. Ma, Z. Tang, W. Feng, Y. Zhang, T.P. Russell, F. Liu, Single-layered organic photovoltaics with double cascading charge transport pathways: 18% efficiencies, *Nat. Commun.* 12 (1) (2021) 309.
- [8] C.M. Sutter-Fella, D.W. Miller, Q.P. Ngo, E.T. Roe, F.M. Toma, I.D. Sharp, M. C. Lonergan, A. Jaye, Band tailing and deep defect states in CH3NH3Pb(I1-xBrx)3 Perovskites as revealed by Sub-bandgap photocurrent, *ACS Energy Lett.* 2 (3) (2017) 709–715.
- [9] J.-P. Yang, F. Bussolotti, S. Kera, N. Ueno, Origin and role of gap states in organic semiconductor studied by UPS: as the nature of organic molecular crystals, *J. Phys. Appl. Phys.* 50 (42) (2017).
- [10] J.-P. Yang, L.-T. Shang, F. Bussolotti, L.-W. Cheng, W.-Q. Wang, X.-H. Zeng, S. Kera, Y.-Q. Li, J.-X. Tang, N. Ueno, Fermi-level pinning appears upon weak electrode-organic contact without gap states: a universal phenomenon, *Org. Electron.* 48 (2017) 172–178.
- [11] S. Olthof, S. Mehraeen, S.K. Mohapatra, S. Barlow, V. Coropceanu, J.L. Bredas, S. R. Marder, A. Kahn, Ultralow doping in organic semiconductors: evidence of trap filling, *Phys. Rev. Lett.* 109 (17) (2012) 176601.
- [12] Y. Kim, A.M. Ballantyne, J. Nelson, D.D.C. Bradley, Effects of thickness and thermal annealing of the PEDOT:PSS layer on the performance of polymer solar cells, *Org. Electron.* 10 (1) (2009) 205–209.
- [13] K. Kawano, R. Pacios, D. Poplavskyy, J. Nelson, D.D.C. Bradley, J.R. Durrant, Degradation of organic solar cells due to air exposure, *Sol. Energy Mater. Sol. Cell.* 90 (20) (2006) 3520–3530.
- [14] Z. Zheng, Q. Hu, S. Zhang, D. Zhang, J. Wang, S. Xie, R. Wang, Y. Qin, W. Li, L. Hong, N. Liang, F. Liu, Y. Zhang, Z. Wei, Z. Tang, T.P. Russell, J. Hou, H. Zhou, A highly efficient non-fullerene organic solar cell with a fill factor over 0.80 Enabled by a Fine-Tuned hole-transporting layer, *Adv. Mater.* 30 (34) (2018) 1801801.
- [15] Y. Guo, H. Lei, L. Xiong, B. Li, Z. Chen, J. Wen, G. Yang, G. Li, G. Fang, Single phase, high hole mobility Cu2O films as an efficient and robust hole transporting layer for organic solar cells, *J. Mater. Chem. A* 5 (22) (2017) 11055–11062.
- [16] X. Wang, P. Liu, B. Yap, R. Xia, W.-Y. Wong, Z. He, High-quality WS2 film as a hole transport layer in high-efficiency non-fullerene organic solar cells, *Nanoscale* 13 (39) (2021) 16589–16597.
- [17] C. Huang, S. Shi, H. Yu, Work function adjustment of Nb2CTx Nanoflakes as hole and electron transport layers in organic solar cells by controlling surface functional groups, *ACS Energy Lett.* 6 (10) (2021) 3464–3472.
- [18] C. Feng, X. Wang, Z. He, Y. Cao, Formation mechanism of PFN dipole interlayer in organic solar cells, *Sol. RRL* 5 (4) (2021) 2000753.
- [19] S. Zhong, R. Wang, H. Ying Mao, Z. He, H. Wu, W. Chen, Y. Cao, Interface investigation of the alcohol-/water-soluble conjugated polymer PFN as cathode interfacial layer in organic solar cells, *J. Appl. Phys.* 114 (11) (2013).
- [20] Z. He, X. Wang, W. Xu, Y. Zhou, Y. Sheng, Y. Rong, J.M. Smith, J.H. Warner, Revealing defect-state photoluminescence in monolayer WS2 by Cryogenic laser processing, *ACS Nano* 10 (6) (2016) 5847–5855.
- [21] Y. Liu, X. Zheng, H. Li, Z. Xu, T. Jiang, Modification of degenerative photoluminescence in aged monolayer WS2 by PC6:BM surface processing, *Appl. Opt.* 56 (4) (2017) 890–896.
- [22] I. Fraga Domínguez, A. Distler, L. Lüer, Stability of organic solar cells: the influence of Nanostructured Carbon materials, *Adv. Energy Mater.* 7 (10) (2017).
- [23] L. Wu, J. Huang, Y. Xie, L. Hong, R. Peng, W. Song, L. Huang, L. Zhu, W. Bi, Z. Ge, Significant efficiency improvement enabled by CdSe/ZnS quantum Dot modifier in organic solar cells, *Sol. RRL* 3 (8) (2019).
- [24] K. Pandi, K. Peramaiah, B. Neppolian, A light soaking free solution processable Metal Oxide cathode interfacial layer Enables high efficiency in bulk heterojunction polymer solar cells, *ACS Appl. Energy Mater.* 4 (10) (2021) 11480–11487.
- [25] Y. Han, H. Dong, W. Pan, B. Liu, X. Chen, R. Huang, Z. Li, F. Li, Q. Luo, J. Zhang, Z. Wei, C.Q. Ma, An efficiency of 16.46% and a T80 lifetime of over 4000 h for the PM6:Y6 inverted organic solar cells enabled by surface acid treatment of the Zinc Oxide electron transporting layer, *ACS Appl. Mater. Interfaces* 13 (15) (2021) 17869–17881.
- [26] R. Peng, T. Yan, J. Chen, S. Yang, Z. Ge, M. Wang, Passivating Surface Defects of N-SnO2 Electron Transporting Layer by InP/ZnS Quantum Dots: toward Efficient and Stable Organic Solar Cells, vol. 6, 2020 1901245, 3.
- [27] W. Yang, W. Wang, Y. Wang, R. Sun, J. Guo, H. Li, M. Shi, J. Guo, Y. Wu, T. Wang, G. Lu, C.J. Brabec, Y. Li, J. Min, Balancing the efficiency, stability, and cost potential for organic solar cells via a new figure of merit, *Joule* 5 (5) (2021) 1209–1230.
- [28] T. Heumueller, T.M. Burke, W.R. Mateker, I.T. Sachs-Quintana, K. Vandewal, C. J. Brabec, M.D. McGehee, Disorder-induced open-circuit voltage losses in organic solar cells during photoinduced Burn-in, *Adv. Energy Mater.* 5 (14) (2015).
- [29] W. Tress, M. Yavari, K. Domanski, P. Yadav, B. Niesen, J.P. Correa Baena, A. Hagfeldt, M. Graetzel, Interpretation and evolution of open-circuit voltage, recombination, ideality factor and subgap defect states during reversible light-soaking and irreversible degradation of perovskite solar cells, *Energy Environ. Sci.* 11 (1) (2018) 151–165.
- [30] J. Kublitski, A. Hofacker, B.K. Boroujeni, J. Benduhn, V.C. Nikolis, C. Kaiser, D. Spoltore, H. Kleemann, A. Fischer, F. Ellinger, K. Vandewal, K. Leo, Reverse dark current in organic photodetectors and the major role of traps as source of noise, *Nat. Commun.* 12 (1) (2021) 551.
- [31] T. Kirchartz, F. Deledalle, P.S. Tuladhar, J.R. Durrant, J. Nelson, On the differences between dark and light ideality factor in polymer:fullerene solar cells, *J. Phys. Chem. Lett.* 4 (14) (2013) 2371–2376.
- [32] G. Garcia-Belmonte, A. Munar, E.M. Barea, J. Bisquert, I. Ugarte, R. Pacios, Charge carrier mobility and lifetime of organic bulk heterojunctions analyzed by impedance spectroscopy, *Org. Electron.* 9 (5) (2008) 847–851.

- [33] E.-P. Yao, C.-C. Chen, J. Gao, Y. Liu, Q. Chen, M. Cai, W.-C. Hsu, Z. Hong, G. Li, Y. Yang, The study of solvent additive effects in efficient polymer photovoltaics via impedance spectroscopy, *Sol. Energy Mater. Sol. Cell.* 130 (2014) 20–26.
- [34] Y.B. Lin, Y. Firdaus, F.H. Isikgor, M.I. Nugraha, E. Yengel, G.T. Harrison, R. Hallani, A. El-Labban, H. Faber, C. Ma, X.P. Zheng, A. Subbiah, C.T. Howells, O. M. Bakr, I. McCulloch, S. De Wolf, L. Tsetseris, T.D. Anthopoulos, Self-assembled monolayer Enables hole transport layer-free organic solar cells with 18% efficiency and improved operational stability, *ACS Energy Lett.* 5 (9) (2020) 2935–2944.
- [35] O. Oklobia, S. Komilian, T. Sadat-Shafai, Impedance spectroscopy and capacitance - voltage measurements analysis: impact of charge carrier lifetimes and mapping vertical segregation in bulk heterojunction P3HT: PCBM solar cells, *Org. Electron.* 61 (2018) 276–281.
- [36] B.R. Weinberger, C.B. Roxlo, S. Etemad, G.L. Baker, J. Orenstein, Optical absorption in Polyacetylene: a Direct measurement using photothermal deflection spectroscopy, *Phys. Rev. Lett.* 53 (1) (1984) 86–89.
- [37] M. Vanecak, A. Poruba, Fourier-transform photocurrent spectroscopy of microcrystalline silicon for solar cells, *Appl. Phys. Lett.* 80 (5) (2002) 719–721.
- [38] J. Nelson, Diffusion-limited recombination in polymer-fullerene blends and its influence on photocurrent collection, *Phys. Rev. B* 67 (15) (2003).
- [39] V.I. Arkhipov, E.V. Emelianova, P. Heremans, H. Bässler, Analytic model of carrier mobility in doped disordered organic semiconductors, *Phys. Rev. B* 72 (23) (2005).
- [40] R.A. Street, K.W. Song, J.E. Northrup, S. Cowan, Photoconductivity measurements of the electronic structure of organic solar cells, *Phys. Rev. B* 83 (16) (2011).
- [41] J.C. Blakesley, D. Neher, Relationship between energetic disorder and open-circuit voltage in bulk heterojunction organic solar cells, *Phys. Rev. B* 84 (7) (2011).
- [42] F. Urbach, The long-Wavelength edge of Photographic Sensitivity and of the electronic absorption of Solids, *Phys. Rev.* 92 (5) (1953), 1324–1324.
- [43] K. Vandewal, K. Tvingstedt, A. Gadisa, O. Inganäs, J.V. Manca, Relating the open-circuit voltage to interface molecular properties of donor:acceptor bulk heterojunction solar cells, *Phys. Rev. B* 81 (12) (2010).
- [44] T.A. Dela Peña, J.I. Khan, N. Chaturvedi, R. Ma, Z. Xing, J. Gorenflo, A. Sharma, F. L. Ng, D. Baran, H. Yan, F. Laquai, K.S. Wong, Understanding the charge transfer state and energy loss trade-offs in non-fullerene-based organic solar cells, *ACS Energy Lett.* 6 (10) (2021) 3408–3416.
- [45] V.I. Arkhipov, P. Heremans, E.V. Emelianova, G.J. Adriaenssens, H. Bassler, Weak-field carrier hopping in disordered organic semiconductors: the effects of deep traps and partly filled density-of-states distribution, *J. Phys. Condens. Matter* 14 (42) (2002) 9899–9911.
- [46] G. Horowitz, M.E. Hajlaoui, R. Hajlaoui, Temperature and gate voltage dependence of hole mobility in polycrystalline oligothiophene thin film transistors, *J. Appl. Phys.* 87 (9) (2000) 4456–4463.
- [47] F. Qiu, Y. Dong, J. Liu, Y. Sun, H. Geng, H. Zhang, D. Zhu, X. Shi, J. Liu, J. Zhang, S. Ai, L. Jiang, Asymmetric organic semiconductors for high performance single crystalline field-effect transistors with low activation energy, *J. Mater. Chem. C* 8 (18) (2020) 6006–6012.
- [48] U. Rau, B. Blank, T.C.M. Müller, T. Kirchartz, Efficiency potential of photovoltaic materials and devices unveiled by detailed-balance analysis, *Phys. Rev. Appl.* 7 (4) (2017).
- [49] J. Yao, T. Kirchartz, M.S. Vezie, M.A. Faist, W. Gong, Z. He, H. Wu, J. Troughton, T. Watson, D. Bryant, J. Nelson, Quantifying losses in open-circuit voltage in solution-Processable solar cells, *Phys. Rev. Appl.* 4 (1) (2015).
- [50] X. Wang, P. Liu, B. Yap, R. Xia, W.Y. Wong, Z. He, High-quality WS<sub>2</sub> film as a hole transport layer in high-efficiency non-fullerene organic solar cells, *Nanoscale* 13 (39) (2021) 16589–16597.
- [51] T. Walter, R. Herberholz, C. Müller, H.W. Schock, Determination of defect distributions from admittance measurements and application to Cu(In,Ga)Se<sub>2</sub>based heterojunctions, *J. Appl. Phys.* 80 (8) (1996) 4411–4420.
- [52] R.A. Street, Y. Yang, B.C. Thompson, I. McCulloch, Capacitance spectroscopy of light induced trap states in organic solar cells, *J. Phys. Chem. C* 120 (39) (2016) 22169–22178.